Process Safety and Environmental Protection 175 (2023) 1–16

Contents lists available at ScienceDirect

Process Safety and Environmental Protection

journal homepage: www.journals.elsevier.com/process-safety-and-environmental-protection

Prediction of BLEVE loading on a rigid structure

Yang Wang [a], Hong Hao [b,a,*], Wensu Chen [a,**], Jingde Li [c], Zitong Wang [a]

[a] Centre for Infrastructural Monitoring and Protection, School of Civil and Mechanical Engineering, Curtin University, Australia
[b] Earthquake Engineering Research & Test Center, Guangzhou University, China
[c] Aspec Engineering Pty Ltd, Perth, Australia

ARTICLE INFO

Keywords:
BLEVE
Reflected overpressure
Reflection coefficient
Diffraction
Clearing time
Reflected impulse

ABSTRACT

Boiling Liquid Expanding Vapour Explosion (BLEVE) in open space has been investigated in the authors' previous study. However, for designing structures against BLEVE event, BLEVE load acting on structures, instead of the pressure in open space, should be used in the structural response analysis. Therefore, further study is required to accurately predict BLEVE loads on structures. In this study, 1300 sets of BLEVE cases consisting of 650 wave propagation in open space and 650 pressure wave-structure interaction cases are numerically modelled. The open space BLEVE pressure and reflected pressure waves from the rigid structure are simulated, and the corresponding impulses are calculated. The reflection coefficient chart is developed to predict the reflected BLEVE overpressure on the rigid structure. The diffraction and clearing effects on the reflected waves are analysed with respect to the dimensions of the structure. An empirical formula for predicting the reflected impulse is also proposed. The results obtained in this study can be used together with the open space BLEVE pressure predictions presented by the authors in a previous study to predict the BLEVE loads on structures.

1. Introduction

Structures exposed to explosions need to be designed for personnel and structure protection. Without proper protective design, a structure might suffer catastrophic damage under explosion loads. For effective and economic structure design, accurate prediction of blast loads is essential, but the loading prediction is not straightforward in practice. To obtain accurate blast loads on structures, the factors such as explosive type, weight and shape of explosive, location between explosive and structure, and the interaction of blast wave with structure and ground need to be considered. These factors determine the amplitude and distribution of blast loads (Hao et al., 2016).

The prediction of blast loads on structures from high explosive detonations has been intensively investigated. The empirical formulae and charts for blast load predictions have been provided in the design manuals, such as the Unified Facilities Criteria UFC-3–340–02 (UFC, 2008). Besides high explosive detonations, accidental gas explosions, such as Vapour Cloud Explosions (VCEs) and Boiling Liquid Expanding Vapour Explosions (BLEVEs), have been occurring around the world and caused significant loss of life and damage to the economy. Various civilian structures (e.g., buildings, bridges, tunnels and highways) and onshore/offshore facilities might be subjected to BLEVE loads induced by LPG or LNG, which could occur during transportation, processing and storage and cause damages to structures (Bariha et al., 2017; Li and Hao, 2021). One of the devastating BLEVE events was the 2018 accident in Bologna, Italy, where a traffic accident involving an LPG truck on a highway bridge led to a BLEVE, which caused at least 3 deaths, 67 injuries, and the partial collapse of the bridge (CNN-news, 2018). In 2005, multiple BLEVEs occurred at the Texas City Refinery (i.e., onshore/offshore facility) due to the overfilling of an isobutene sphere tank, which led to explosions in a tank farm. The main cause of the accident was the failure of a pressure control valve and a high-level alarm defector, resulting in severe damage to the refinery and surrounding areas. This accident resulted in 15 fatalities, over 180 injuries, and millions of dollars in losses, with the entire isomerization process unit being out of operation for more than two years (CSB, 2008). Such explosions can also generate debris, which can pose a significant risk to individuals and properties in the vicinity. Hence, it is essential to accurately predict the blast loads generated by BLEVE for effective structural designs to resist such loads.

BLEVEs occur when the pressurized tank ruptures suddenly and the internal liquid temperature exceeds its boiling point. Based on the

* Corresponding author at: Centre for Infrastructural Monitoring and Protection, School of Civil and Mechanical Engineering, Curtin University, Australia.
** Corresponding author.
E-mail addresses: hong.hao@curtin.edu.au (H. Hao), wensu.chen@curtin.edu.au (W. Chen).

https://doi.org/10.1016/j.psep.2023.04.049
Received 28 December 2022; Received in revised form 13 March 2023; Accepted 28 April 2023
Available online 4 May 2023
0957-5820/© 2023 The Author(s). Published by Elsevier Ltd on behalf of Institution of Chemical Engineers. This is an open access article under the CC BY-NC-ND license (http://creativecommons.org/licenses/by-nc-nd/4.0/).

failure conditions (i.e., failure temperature and pressure), BLEVEs can be classified into "non-superheated" and "superheated". A temperature limit, named 'superheat limit temperature (SLT)', is defined as the temperature exceeding the normal boiling point of liquid at atmospheric pressure without boiling and cannot make the liquid superheated (CCPS, 2011; Ustolin et al., 2022). Non-superheated BLEVEs occur when the failure temperature is between the ambient boiling point and SLT. Only vapour expansion is taken into account in the energy calculation. Superheated BLEVEs occur when the failure temperature is higher than SLT. At the initial stage, the bubble nuclei are very small and thus more superheat is required to grow the bubble nuclei (CCPS, 2011). When the liquid temperature is significantly higher than SLT under ambient pressure, homogeneous nucleation and evaporation can occur rapidly. Heat resulting from the liquid is used for nucleation and vaporization. During this process, a very violent phase transition occurs (i.e., the liquid phase instantly changes to the vapour phase). That is, the energy from liquid flashing also contributes to the formation of the blast waves along with the vapour expansion energy (CCPS, 2011; Eckhoff, 2014).

Compared to high explosive detonations with the same released energy, gas explosions usually generate lower peak overpressure, slower pressure rising, longer duration and higher impulse (Hao et al., 2016). Therefore, the design against gas explosions such as BLEVE differs from that against TNT explosions. Energy equivalence methods and numerical simulations based on Computational Fluid Dynamics (CFD) modelling have been used to predict BLEVE loads. Energy equivalence methods use theoretical-based empirical models derived from various thermodynamics assumptions and energy laws. Using equivalent high explosives to predict gas explosions, such as BLEVEs, could result in an inaccurate prediction of loading profile (Wang et al., 2022a). For example, the loading duration predicted by using the TNT-equivalence method is very short and much smaller than the vibration period of the structure and structural components, while the actual BLEVE loading duration is in an order of tens of milliseconds, which could be comparable to the vibration period of structural components such as columns, hence using blast load predicted by TNT-equivalence method may lead to inaccurate predictions of structural responses induced by BLEVE loads. CFD numerical simulations can more accurately predict the loads, and the reliable BLEVE prediction models have been developed by Hansen and Kjellander (2016), Hutama (2017) and Li and Hao (2020).

Based on the CFD numerical simulations, Li et al. (2021) and Wang et al. (2022b) developed the fast Artificial Neural Network (ANN) model and easy-to-use empirical models for the BLEVEs occurred in open space. The ANN method is a data-driven computation model that learns from training data. A properly trained ANN model can reduce human errors and perform high-speed calculations, achieving a balance of prediction accuracy and efficiency. However, the available data for training the network is limited, which can result in overfitting or underfitting of the model, leading to inaccurate predictions or poor generalization to new cases. Meanwhile, the accuracy of the ANN model heavily relies on the quality of training data mainly calculated from the empirical or CFD models as actual testing data are very limited, which inherit their weaknesses. Additionally, the ANN functions cannot be directly used like empirical models. As a result, the authors further proposed empirical models for BLEVE pressure prediction in open space (Wang et al., 2022b), enabling engineers to make predictions more easily. Empirical formulae and charts on pressure-time profiles are derived for two types of medium-to-large-scaled BLEVEs (i.e., non-superheated and superheated) in open space, including positive and negative side-on peak overpressure, positive and negative duration, arrival time, positive and negative peak pressure rise time and impulse (Wang et al., 2022b). For structural design, the blast load acting on structures, which is different to the pressure in open space, should be used. BLEVE load on structures is more complicated than that in open space due to the interaction between the blast wave and structures, which is affected by the blast wave velocity, angle of incidence, structural dimensions and stiffness, etc. It should be noted that the size of the structure significantly affects the diffraction and pressure relief of blast waves. When the dimension of structure is small, a portion of blast waves are diffracted from the side and top walls, increasing the blast wave intensity behind the structure. When the structure is large, the diffracted pressure wave is insignificant, and blast waves are completely reflected. The blast wave's intensity at the structure's rear wall is greatly attenuated by weak diffraction (Shi et al., 2007).

Table 1
Details of large-scale BLEVE experiments (Balke et al., 1999; Johnson and Pritchard, 1990; Betteridge and Phillips, 2015).

Experiments	Fluid	P_i [bar]	Status	Liquid ratio [%]	V [m^3]	r [m]
BAM (Balke et al., 1999)	Propane	25	Superheated	22	45.36	100/150
Johnson and Pritchard (1990)	Propane	15	Non-superheated	80	5.659	150
	Butane	14.6	Non-superheated	75	5.659	25
	Butane	15.1	Non-superheated	76	5.659	25/50
	Butane	15.1	Non-superheated	40	10.796	25/50
	Butane	15.2	Non-superheated	38/76	5.659	25/50
Betteridge and Phillips (2015)	LNG	13.01	Non-superheated	37	5.055	40/70/100

Note: failure pressure (P_i), BLEVE tank volume (V), and distance between the BLEVE and target (r)

By extending the authors' previous work in open space (Wang et al., 2022a), this study predicts the BLEVE loads on a rigid structure, in particular the pressure profile at the centre point in front of the structure, which can be used to better analysis of structural responses to BLEVE load. To simplify the analysis, the structure in this study is assumed as rigid. Based on the 1300 sets of BLEVE cases consisting of 650 in open space and 650 wave-structure interaction cases, BLEVE reflection coefficient chart and empirical formula for reflected impulse are developed to predict blast loads on a rigid structure. Additionally, the BLEVE wave interactions with structures of different dimensions are also discussed to reveal the pressure relief at the free edges of the structure, including the wave diffraction and clearing effect on reflected overpressure. An example is provided to illustrate how to predict the reflected overpressure and impulse on a rigid structure in combination with the authors' previous study in predicting BLEVE pressure in open space.

2. Numerical modelling

To predict BLEVE loading on a rigid structure, the numerical modelling needs be employed since the empirical method cannot provide accurate prediction as mentioned above. Numerical models are used to accurately predict the BLEVE generation, wave propagation and interaction with structures to obtain the reflected overpressure on the structure. Commercial software such as ANSYS Fluent and StarCD can simulate the wave propagation and interaction with structure, but they are unable to model the generation of BLEVE. FLACS is thus used in this study as it can simulate the generation of BLEVE, the propagation of waves, and the interaction with structures.

2.1. Validation of CFD models

FLACS is a commonly used CFD commercial software to predict BLEVE. For condensed explosives modelling and blast wave propagation, FLACS-Blast module is employed to compute via Euler euqations,

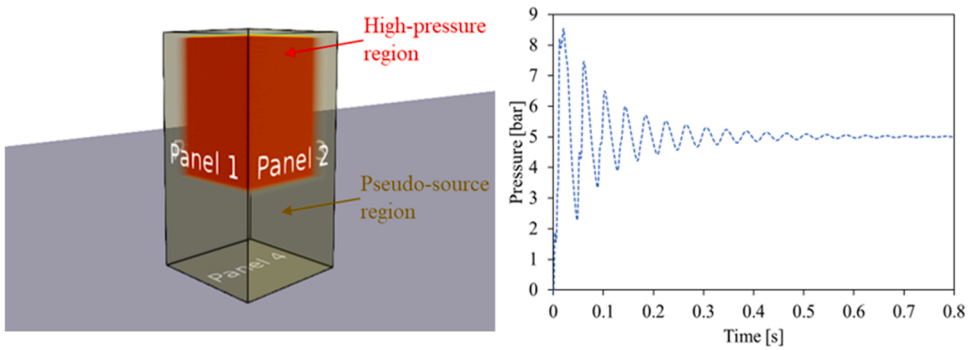

Fig. 1. Pseudo-source simulation: (a) Modelling in FLACS; (b) Pressure time history of monitor point inside the pseudo-source.

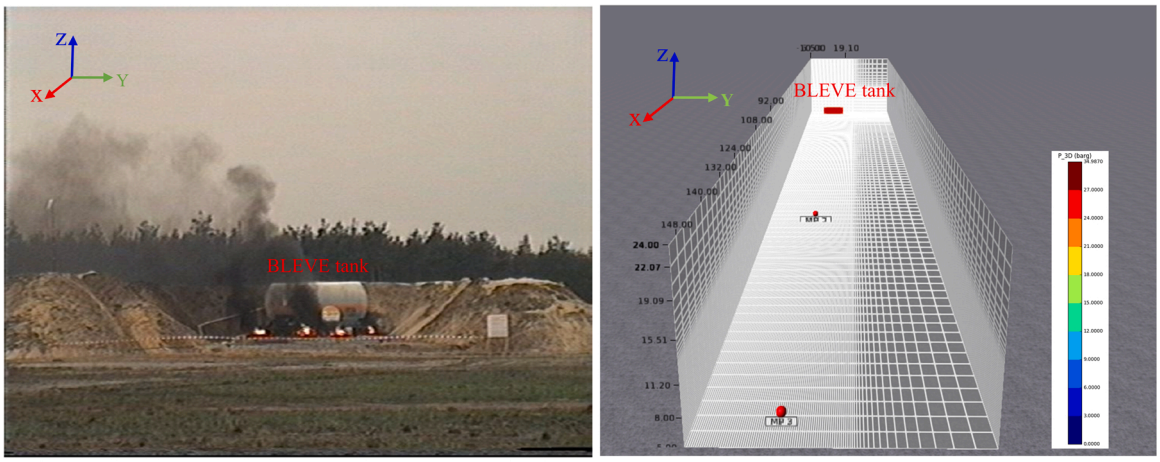

Fig. 2. Large-scale BLEVE experiments: (a) BAM's test (Balke et al., 1999); (b) 3D model in FLACS.

flux-corrected transport (FCT) scheme and a second-order flux correction (Gexcon, 2022). Large-scale experiments are used to calibrate the numerical model, including BAM's tests in Germany (Balke et al., 1999), Johnson and Pritchard's experiments (Johnson and Pritchard, 1990) and Betteridge and Phillips' experiments (Betteridge and Phillips, 2015) from the literature. The experimental details are shown in Table 1, including the pressurized liquid, failure pressure (P_i), failure status, liquid ratio, BLEVE tank volume (V) and the distance between the BLEVE and target (r). Numerical simulations of BLEVEs for both "non-superheated" and "superheated" cases are validated. In terms of non-superheated BLEVE, only vapour expansion provides the energy to generate the first blast wave. If the internal liquid of BLEVE is in the

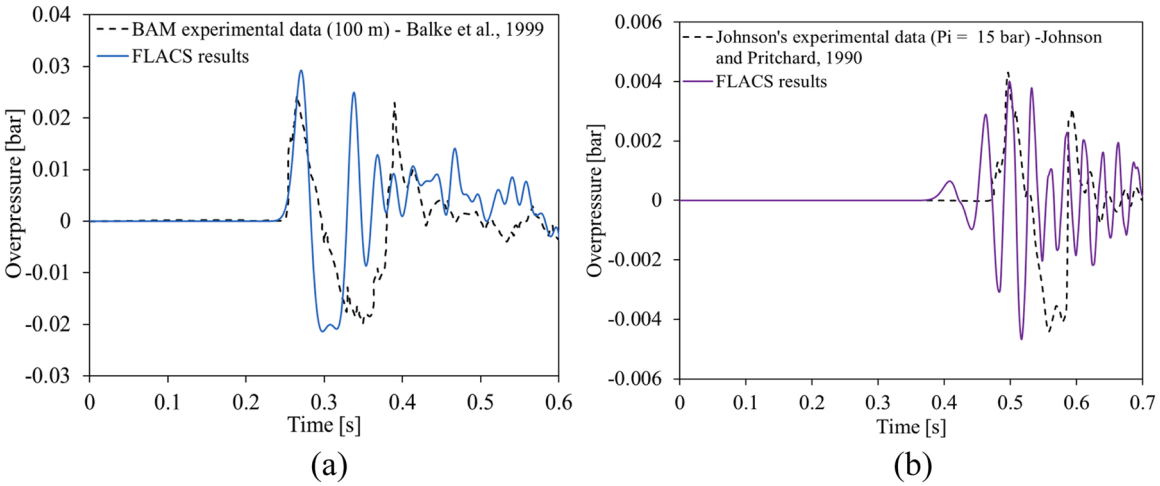

Fig. 3. Pressure time history (numerical results vs experimental data): (a) BAM's experiment (Balke et al., 1999); (b) Johnson's experiment (Johnson and Pritchard, 1990).

Table 2
Performance metrics of numerical results for large-scale BLEVE experiments.

Performance metrics	MG	VG	FAC2	FB	NMSE
Value	0.61 – 1.44	1.00 – 1.29	100%	0.11	0.03

Note: Geometric mean bias (MG), geometric variance (VG), prediction fraction within a factor of two observations (FAC2), fractional bias (FB) and normalized mean square error (NMSE)

superheated status, liquid flashing energy and vapour expansion energy should be considered together for blast wave generation. However, it is unable to model two high-pressure regions (i.e., vapour and liquid phase) in FLACS since it can define only one high-pressure region (Li and Hao, 2020). To accurately simulate BLEVEs under "superheated" status in FLACS, the liquid correction method (Li and Hao, 2020) is applied to calculate the final failure pressure of BLEVE. This method introduces a pseudo-source in the FLACS modelling to simulate the second high-pressure region (i.e., liquid phase). Fig. 1(a) presents the pseudo-source and high-pressure regions of BAM tests, which are fully confined by the panels. When the stable pressure is equal to 20% of tank failure pressure (i.e., 5 bar), the corresponding initial pressure of pseudo-source (i.e., 10 bar) is the BLEVE rupture pressure contributed by flashing liquid (Li and Hao, 2020), as shown in Fig. 1(b). Therefore, the total failure pressure of BAM tests is 35 bar in FLACS simulations. The monitoring points are arranged at the same location as the experimental setup to compare the experimental data and numerical results, as shown in Fig. 2. In numerical simulations, "PLANE_WAVE" boundary conditions are applied to eliminate the reflection. A uniform grid of 0.2 m is used in the core domain, as this grid size can achieve the balance between accuracy and efficiency (Li and Hao, 2020; Li et al., 2021). Grid size outside the core domain is gradually stretched by a factor of 1.1 to speed up the simulations.

The accuracy of using FLACS in predicting the BLEVE pressure-time profile is illustrated in Fig. 3. BAM's experiment and one of Johnson's experiments (P_i = 15 bar) are used for verifications of BLEVE pressure predictions in "superheated" and "non-superheated" conditions, respectively. As shown, the peak overpressure can be well predicted by FLACS. FLACS overestimates the peak overpressure of BAM by less than 30%. It is worth mentioning that there are multiple oscillating pressure spikes in simulations because the grid cells are stretched to balance the computational accuracy and efficiency due to the large-scale BLEVEs (Li and Hao, 2020).

Multiple performance metrics are used to qualitatively evaluate the performance of FLACS simulations, and each metric has its strength and weakness. Five performance metrics include the geometric mean bias (MG), geometric variance (VG), prediction fraction within a factor of two observations (FAC2), fractional bias (FB) and normalized mean square error (NMSE) (Gexcon, 2022). The bias between the results of FLACS simulations (X_p) and experimental data (X_o) can be determined by these metrics, which are defined by Eqs. (1) to (5). As specified in the FLACS-CFD user's manual (Gexcon, 2022), at least 50% of predicted data should be within the range of FAC2 (i.e., FAC2 > 50%), and the bias (FB & MG) requires $-0.67 < FB < 0.67$ or $0.5 < MG < 2.0$, and random scatter (NMSE & VG) should have a value of NMSE < 1.5 or VG < 4. The five-performance metrics of these data are given in Table 2, indicating all numerical results are within the acceptable range.

Additionally, the scatter and parabola plots are shown in Fig. 4, indicating the number of predicted data falling into the "Excellent" region. The scatter plot depicts the excellent deviation range and FAC2 region, indicating the majority of the numerical results have a deviation of less than 30% from the experimental data, and 100% of the predicted results fall into the range of FAC2. Meanwhile, the parabola plot further presents the predictive performance of numerical simulations through systemic overprediction or underprediction (i.e., MG) and scatter of the numerical results (i.e., VG). As shown, most numerical results fall into the "Excellent" region, and all the data are within the "Acceptable" region. Thus, FLACS can accurately predict the peak overpressure resulting from large-scale BLEVEs.

$$MG = \exp\left[\ln\left(\frac{X_p}{X_o}\right)\right] \tag{1}$$

$$VG = \exp\left[\ln\left(\frac{X_p}{X_o}\right)^2\right] \tag{2}$$

$$FAC2 = the\ fraction\ of\ data\ where\ 0.5 \le \frac{X_P}{X_o} \le 2.0 \tag{3}$$

$$FB = \frac{\overline{X}_P - \overline{X}_o}{0.5(\overline{X}_P + \overline{X}_o)} \tag{4}$$

$$NMSE = \frac{\overline{(X_P - X_o)^2}}{\overline{X}_P \overline{X}_o} \tag{5}$$

This study focuses on the BLEVE wave reflected on a rigid structure. Hence, the accuracy of blast wave interaction with a structure should be validated. Since no available BLEVE experiment was conducted in obstructed environments, the reflected and diffracted BLEVE waves

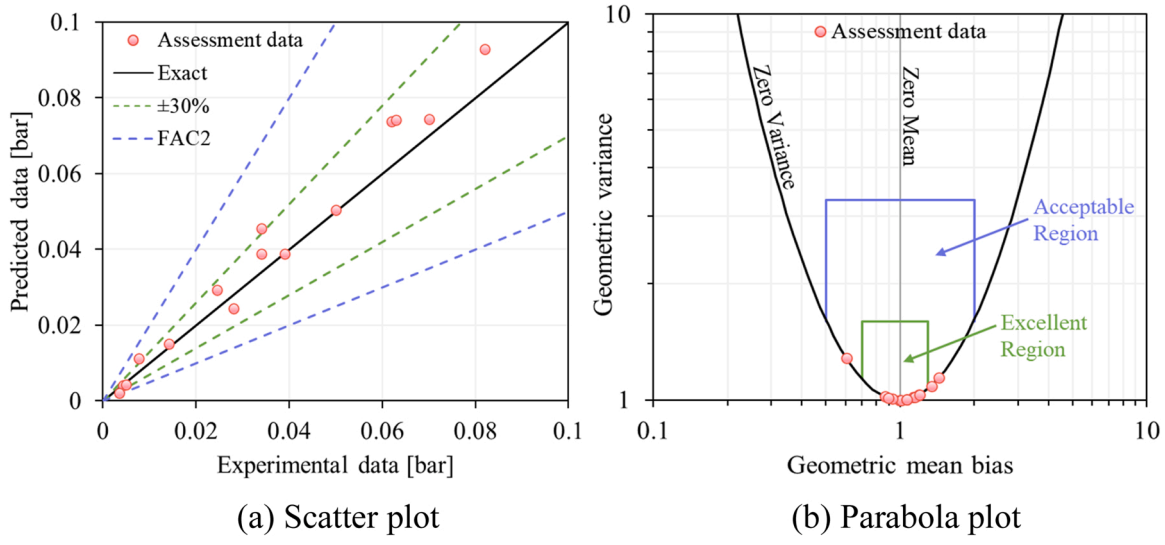

Fig. 4. Comparison of numerical results and experimental data in (a) scatter plot and (b) parabola plot.

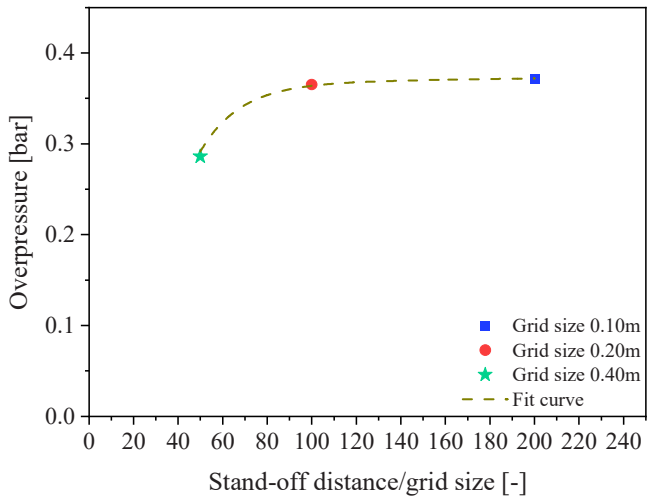

Fig. 5. Grid sensitivity study of BLEVE loads on a rigid structure.

Table 3
Variables of BLEVE simulation (Li et al., 2021).

Variable	Butane	Propane
Tank failure pressure, P_i (bar)	5 – 37	5 – 42
Liquid temperature, T_l (°C)	1 – 152	1 – 96
Vapour temperature, T_v (°C)	1 – 304	1 – 192
Liquid status at failure	Non-superheated or superheated	
Liquid fill level, *LFL* (%)	10 – 90	
Tank width, W_{tank} (m)	0.2 – 3	
Tank length, L_{tank} (m)	0.2 – 10	
Tank height, H_{tank} (m)	0.2 – 3	
Structure width, W_{str} (m)	3 – 18	
Structure thickness, L_{str} (m)	0.4 – 3	
Structure height, H_{str} (m)	3 – 18	
Distance between structure centre and BLEVE centre (m)	0 – 20	
BLEVE height above ground, H_{BLEVE} (m)	0 – 2	
Angle of incidence, α (degree)	0 – 90	

cannot be directly compared with experimental data. However, the accuracy of FLACS in predicting the interaction of blast waves with structures has been demonstrated in previous studies. For instance, Li and Hao (2019) measured the overpressure of vented gas explosions between two tanks in a tank group. The interaction of blast waves and the cylindrical obstacle was simulated to predict the reflected overpressure on the front and rear surfaces of the tank. Numerical simulations achieved reasonable accuracy in predicting overpressure between structure walls as compared to the experimental data, indicating FLACS can model the reflected blast waves well. Liu et al. (2020) performed full-scale gas explosion experiments in an urban regulator station (i.e., vented confined space), and pressure sensors were located outside the door and windows. In addition, the numerical simulation was conducted using FLACS, and the predicted peak overpressure agrees well with the experimental results, proving that FLACS can well capture the wave diffraction. Therefore, the characteristic of blast wave and structure interaction can be well simulated in FLACS.

The grid sensitivity analysis of BLEVE loads on a rigid structure using different grid sizes (i.e., 0.4 m, 0.2 m and 0.1 m) is shown in Fig. 5. A grid size of 0.2 m is the optimal one for achieving a balance of accuracy and computational efficiency. Meanwhile, this grid size is consistent with the authors' previous study (i.e., BLEVE in open space), enabling the same grid setup to be applied in the simulation of BLEVE wave propagation in open space and interaction with a rigid structure.

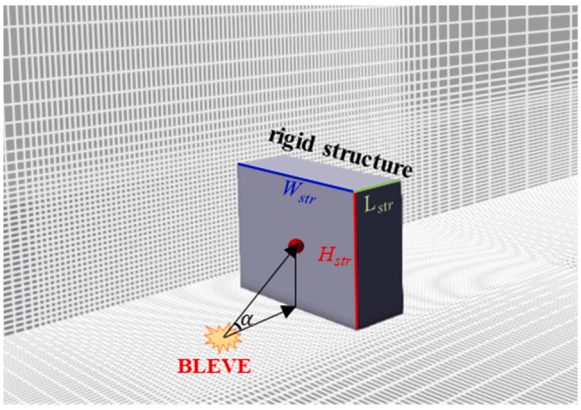

Fig. 6. Schematic diagram of numerical model.

2.2. CFD simulation

After demonstrating the accuracy of FLACS in predicting BLEVE pressures in free air and the pressure wave interaction with structures, the pressure waves from BLEVEs of different conditions in free air and their interactions with a rigid structure of different dimensions are simulated. BLEVE is a complex physical explosion, and many critical parameters affect the BLEVE overpressure and wave propagation, including tank failure pressure, failure temperature, liquid ratio, tank dimensions (i.e., length, width and height) and stand-off distance (Wang et al., 2022b). In this study, 1300 BLEVE cases are simulated, and the simulations are carried out by randomly and uniformly sampling the respective BLEVE parameters. The BLEVE parameters are defined within the practical ranges, as shown in Table 3. BLEVE simulations in open space are carried out first, following the same settings as Li et al. (2021). This study focuses on LPG-induced BLEVEs. Hence, butane and propane are selected as pressurised liquids. BLEVE tank failure conditions are essential to determine the internal liquid status and the BLEVE energy. To consider "non-superheated" and "superheated" BLEVEs, the failure pressure is defined from minimum experimental pressure (i.e., 5 bar) to critical pressure of the pressurised liquid, and the failure temperature is defined up to its critical temperature. The simulations simplify the BLEVE tank as rectangular to minimise the mass residual issue, since FLACS uses the block control volume as the grid meshing (Gexcon, 2022). Based on the European manufacturing standard of LPG tanks, the volume of BLEVE is sampled from 10 m^3 to 90 m^3 (Kadatec, 2017). When the propagating BLEVE pressure wave arrives at a rigid rectangular structure, the interaction of the pressure wave with the structure causes wave reflection and diffraction depending on the wave amplitude, velocity and duration, as well as the structural dimension, geometry and stiffness. As stated above in this study, the structure is assumed as rectangular and rigid, only the dimension is changed. The smallest structural size is 3 m in width, 3 m in height and 0.4 m in thickness, while the largest dimension is 18 m in width, 18 m in height and 3 m in thickness. Usually the maximum reflected overpressure occurs when the blast wave incident angle is perpendicular to the surface of the structure and the minimum when the blast wave incident angle is parallel to the surface of a structure, but this is not necessarily true for shock waves owing to Mach effect and is also incident pressure wave amplitude dependent as indicated in UFC-3–340–02 (UFC, 2008). In this study, the angle of incidence (α) between the BLEVE centre and structure centre is varied from 0° to 90° to investigate the incident angle effect on BLEVE pressure wave reflection. To prevent the smearing of the BLEVE waves, a uniform grid of 0.2 m is applied in the region containing BLEVE sources and the rigid structure. (Fig. 6)

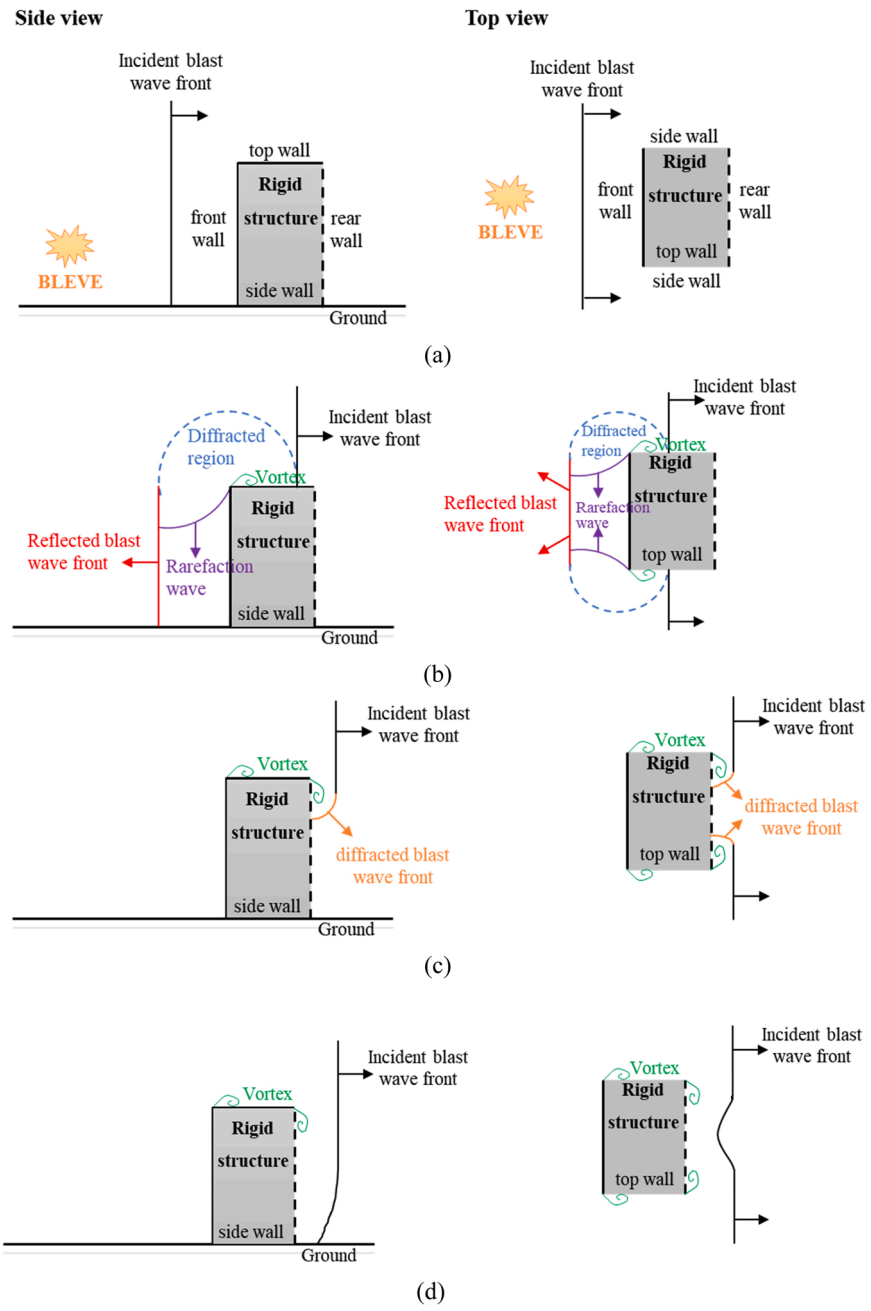

Fig. 7. Schematic top view and side view of BLEVE wave interaction with a rigid structure (ASCE, 2010; Green-Book, 1992): (a) Incident waves at the front surface; (b) Reflected and diffracted waves at the front surface; (c) Diffracted waves at the rear surface; (d) Diffraction complete at the rear surface.

3. Blast wave-structure interaction

With the validated CFD models, the interaction between blast waves and a rigid structure is investigated. The interaction is complicated when blast waves act on a finite-size structure due to wave reflection and diffraction. Fig. 7 shows a schematic diagram of the BLEVE wave interaction with a rigid rectangular structure on the front and rear surfaces from the side and top views. When BLEVE occurs, blast waves propagate outward from the explosion centre, as shown in Fig. 7(a). A reflected wave is formed immediately when the incident wave reaches the target surface. Although a portion of the incident wave is reflected from the target surface, the remaining unblocked incident waves travel along the surface edge, causing a diffraction phenomenon around the free edge. Diffraction generates rarefaction waves, resulting in the pressure imbalance between low-pressure rarefaction waves and high-pressure reflected waves. As the pressure eventually reaches equilibrium, air begins to flow from the high-pressure region to the low-pressure region (i.e., propagates from boundaries to centre) (Rickman and Murrell, 2007; Rigby et al., 2012; Tyas et al., 2011). Fig. 7(b) illustrates the pressure flow on the structure's top and two side walls during the blast wave propagation. Subsequently, diffracted waves travel along the free edges to the rear surface. BLEVE waves envelop the structure after the diffracted wavefront reaches the rear surface of the structure and forms a pair of vortexes around the free edge, as shown in Fig. 7(c). After the diffraction process completes, the blast waves bypass the structure and continue to travel as shown in Fig. 7(d) (ASCE, 2010; Green-Book, 1992). In fact, the reflected wave can deform a non-rigid structure, affecting the reflected peak overpressure and impulse (Shi et al., 2007). However, a rigid structure is assumed in this study, and thus there is no structural deformation. The reflection and diffraction of

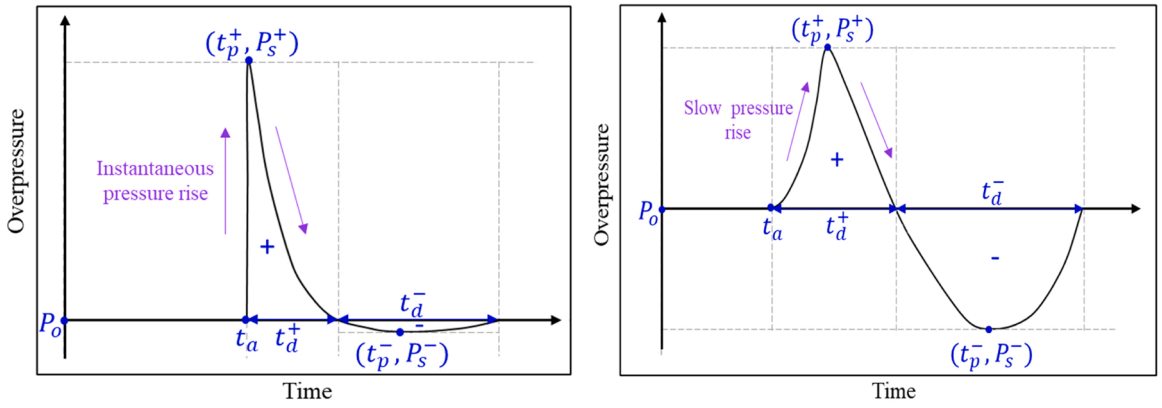

Fig. 8. Typical overpressure-time profiles: (a) TNT explosion; (b) BLEVE. Note: ambient pressure (P_o), positive peak overpressure (P_s^+), negative peak overpressure (P_s^-), arrival time (t_a), positive duration (t_d^+), negative duration (t_d^-), positive peak pressure rise time (t_p^+) and negative peak pressure rise time (t_p^-).

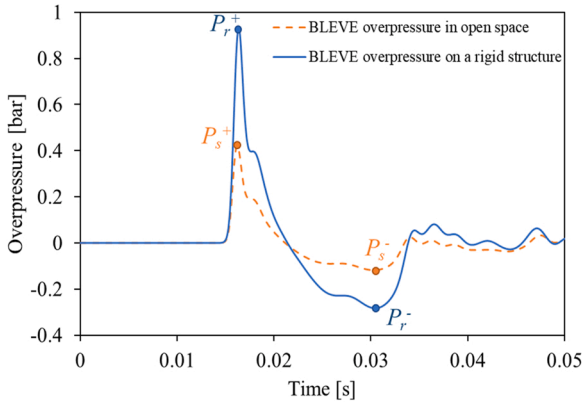

Fig. 9. BLEVE pressure-time profile (P_s: incident peak overpressure & P_r: reflected peak overpressure).

BLEVE waves on rigid structures with different dimensions are discussed in the following sections.

4. Reflected overpressure of BLEVE pressure wave

The phenomenon of BLEVE wave-structure interaction is presented in Section 3. Since the reflected overpressure is the blast load on the structure, this section presents the BLEVE reflected overpressure and the reflection coefficient chart at the centre point of the front wall.

4.1. Reflected overpressure profile

An explosion is defined as a sudden growth in volume and release of energy during a short period, resulting in pressure wave propagation (Ngo et al., 2007). The typical pressure-time profiles of high explosion and BLEVE are shown in Fig. 8. Seven essential parameters to determine the pressure-time profile include arrival time (t_a), positive and negative peak pressure ($P_s^+ \& P_s^-$), positive and negative peak pressure rise time ($t_p^+ \& t_p^-$) and positive and negative duration ($t_d^+ \& t_d^-$). BLEVEs generate a much lower pressure rise rate than high explosive detonations, indicating a less significant loading rate on structure. Meanwhile, BLEVE pressure wave has a longer positive duration than that of high explosive

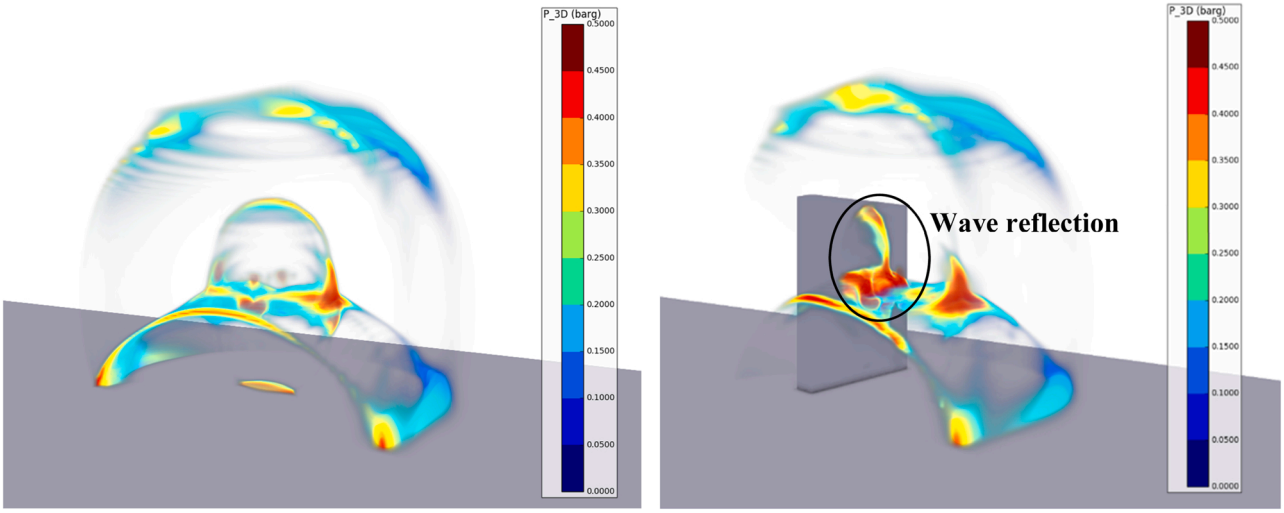

Fig. 10. BLEVE pressure wave propagation: (a) in open space; (b) interaction with a rigid structure.

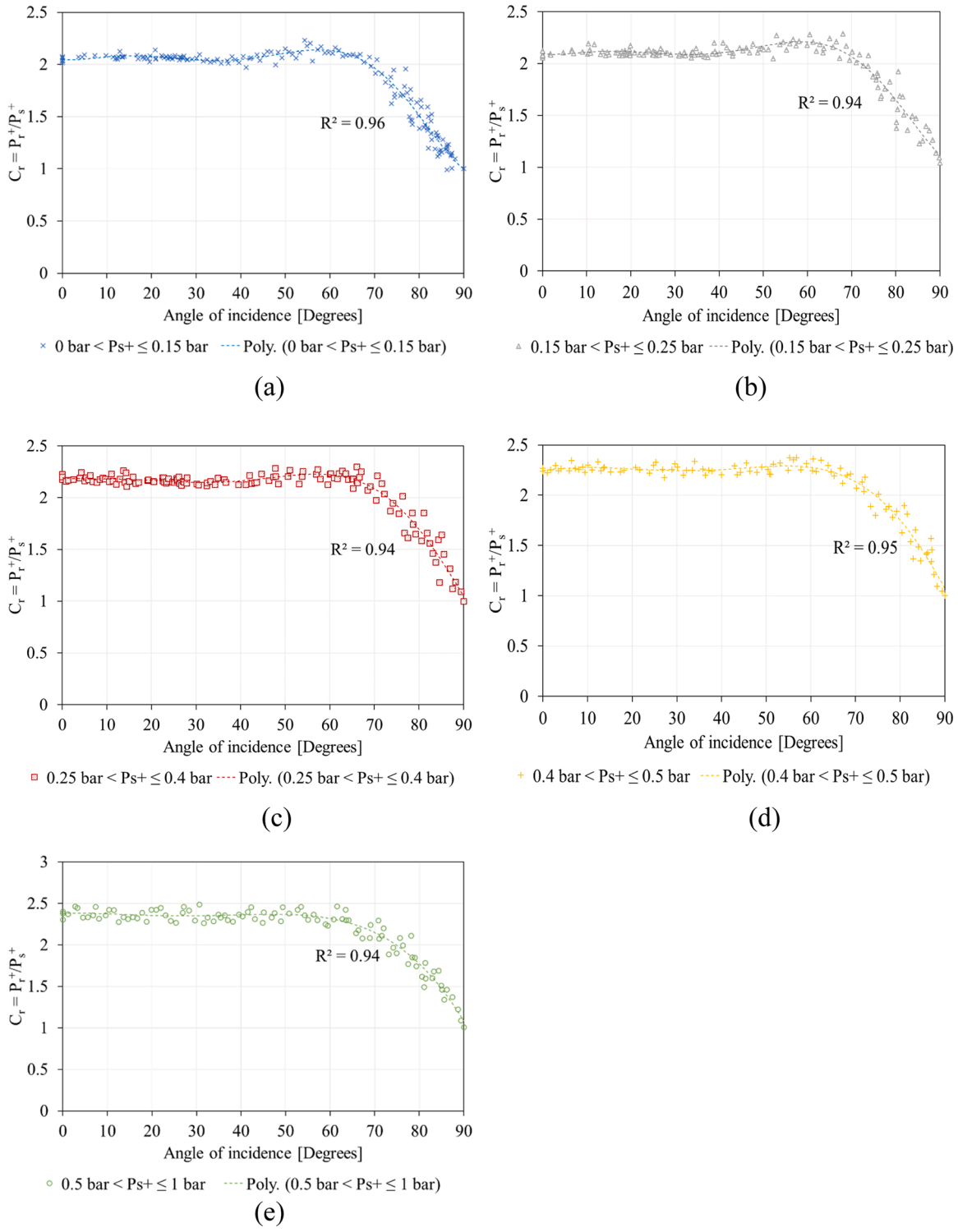

Fig. 11. BLEVE reflection coefficient for positive overpressure (C_r) charts: (a) $0bar < P_s^+ \leq 0.15bar$; (b) $0.15bar < P_s^+ \leq 0.25bar$; (c) $0.25bar < P_s^+ \leq 0.4bar$; (d) $0.4bar < P_s^+ \leq 0.5bar$; (e) $0.5bar < P_s^+ \leq 1bar$.

detonations. For example, the positive pressure duration of a typical TNT explosion is usually in an order of a few milliseconds, e.g., about 5.98 ms for a 1-tonne TNT explosion at a stand-off distance of 13.1 m (Xu et al., 2021). On the contrary, a BLEVE pressure wave has a relatively long duration. For instance, the duration generated by BLEVE from a 2 m^3 tank with a 51% liquid ratio is approximately 25 ms at stand-off distance 20 m (Birk et al., 2007). Longer duration usually leads to higher impulse. Therefore, proper modelling of the BLEVE pressure waves is essential for accurately defining the BLEVE loads on structures.

When a BLEVE occurs in front of a rigid structure, the propagating pressure wave interacts with the structure and generates blast load on the structure. Due to the interaction between the BLEVE waves and the structure, a portion of the blast waves is reflected from the front surface. The superposition of the reflected overpressure and incident overpressure intensifies the blast overpressure. As compared with BLEVE overpressure in open space, both positive and negative peak over-

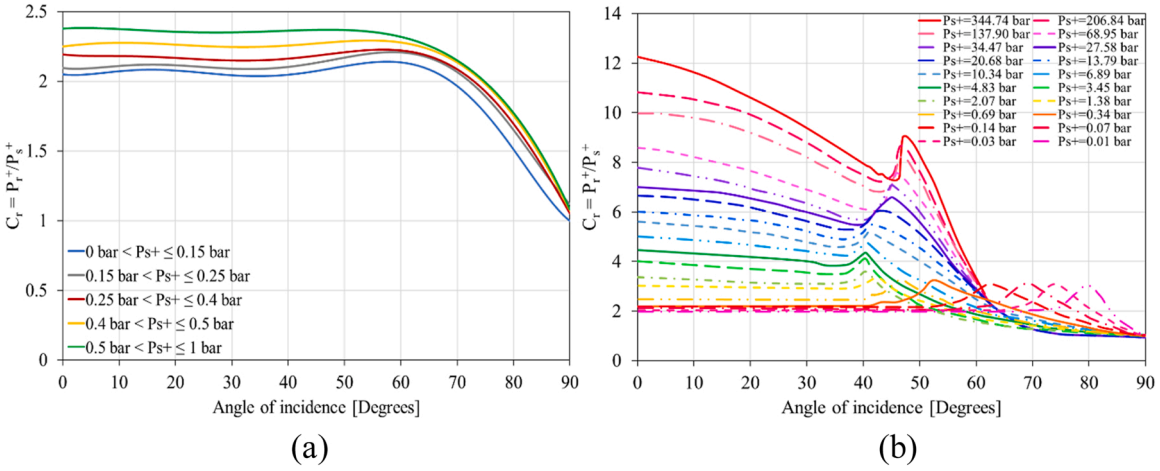

Fig. 12. Comparison of reflection coefficient for positive overpressure (C_r) charts: (a) BLEVEs (incident overpressure ≤ 1 bar); (b) TNT explosions (UFC, 2008).

pressures of BLEVE on a rigid structure are amplified while other essential parameters (t_a, t_d^+, t_d^-, t_p^+ & t_p^-) are less affected, as shown in Fig. 9. The reflected overpressure in the CFD model is shown in Fig. 10 when the BLEVE wave propagates to a rigid structure. The relationship between reflected overpressure and incident overpressure (i.e., reflection coefficient) is affected by explosive conditions (e.g., type and weight), stand-off distance, location between charge and structure, structure configuration (e.g., geometry and dimension), the interaction of blast wave with structure and ground, etc. (Karlos and Solomos, 2013). High explosive detonation is a chemical explosion and the incident overpressure is mainly determined by the stand-off distance and charge weight. However, BLEVE is a physical explosion, more factors affect the explosion incident overpressure due to the co-existence of vapour and liquid in the BLEVE tank. Hence, the explosion conditions of BLEVE are more complicated since the tank failure pressure, failure temperature, liquid ratio, and tank dimensions (i.e., width, length and height) all affect BLEVE pressures. Therefore, the effects of different factors on the BLEVE should be considered. That is, explosion scenarios with different initial conditions need to be investigated along with different incidence angles between the explosive and structure besides the equivalent explosion energy, structure configuration and stand-off distance.

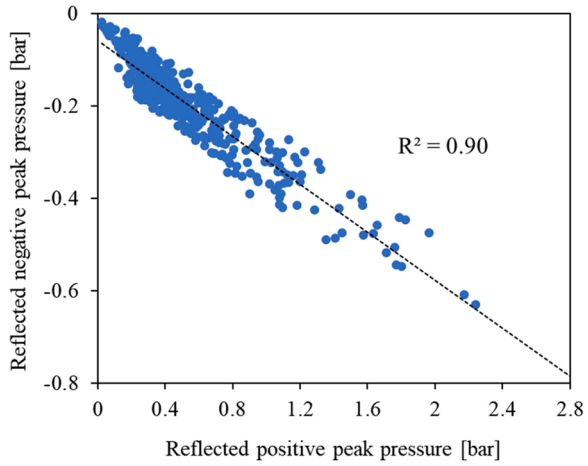

Fig. 13. Correlation between reflected negative peak pressure (P_r^-) and reflected positive peak pressure (P_r^+).

4.2. Reflection coefficient (C_r) for positive overpressure (P_r^+)

As mentioned above, the reflected peak overpressure may be several times higher than the incident peak overpressure (Karlos and Solomos, 2013). The reflected peak overpressure can vary widely based on the incident peak overpressure, and the relative angle from the BLEVE centre to the structure centre. Incident peak overpressure is mainly affected by the stand-off distance between BLEVE and structure as well as the BLEVE initial conditions, such as BLEVE failure conditions (i.e., failure pressure and temperature), liquid ratio, and tank dimensions (i.e., width, length and height). Angle of incidence (α) is another essential parameter that has a significant effect on reflection. When the propagation direction of the blast wave is perpendicular to the surface (i.e., $\alpha = 0°$), the highest reflected overpressure is generated when Mach stem is not formed. When the direction of the reflected pressure wave is parallel to the surface (i.e., $\alpha = 90°$), the reflected pressure is equal to the incident pressure. The ratio of the peak reflected overpressure (P_r^+) to the incident peak overpressure (P_s^+) is defined as the reflection coefficient as expressed in Eq. (6).

$$C_r = \frac{P_r^+}{P_s^+} \tag{6}$$

A total of 1300 sets of BLEVE cases (i.e., 650 in open space and 650 pressure wave and rigid structure interaction cases) are used to derive the BLEVE reflection coefficients. Fig. 11 shows the BLEVE reflection coefficient charts based on different ranges of incident overpressure, including $0bar < P_s^+ \leq 0.15bar$, $0.15bar < P_s^+ \leq 0.25bar$, $0.25bar < P_s^+ \leq 0.4bar$, $0.4bar < P_s^+ \leq 0.5bar$ and $0.5bar < P_s^+ \leq 1bar$, respectively. The R-square values are over 0.94 for all reflection coefficient charts of BLEVE, indicating good fitting results.

As shown in Fig. 11, the reflection coefficient decreases in general as the angle of incidence increases from 0 to 90 degrees. However, the reflection coefficient of BLEVE has a very slight increase in the range of the angle of incidence from 50° to 70°. Fig. 12 compares the reflection coefficient of TNT explosions and BLEVEs. Compared to the BLEVE reflection coefficient chart, the reflection coefficient from a TNT explosion increases rapidly when reaching the critical angle of incidence. The sudden increase in reflected overpressure is due to the incident blast wave heating the air as it passes through. The reflected waves have a faster propagation speed and eventually catch up with the incident blast waves (Janney, 2007). At the critical angle of incidence, the reflected wave catches up and merges with the incident wave to form a Mach stem, which is the transition point from regular to Mach-reflected shock waves (Johnson-Yurchak, 2020; Shin et al., 2017). The Mach stem can greatly intensify the overpressure (Rigby et al., 2015).

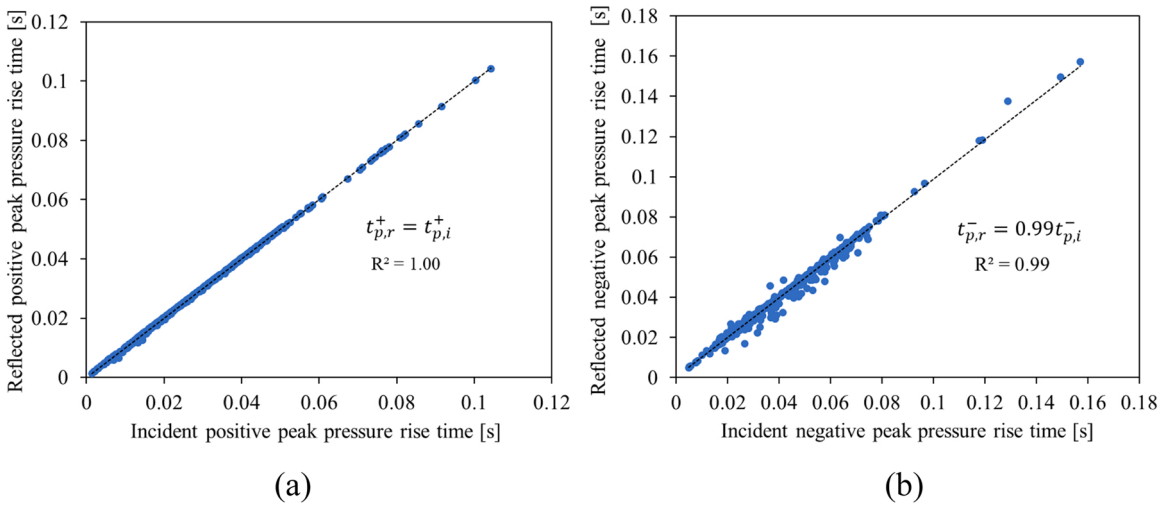

Fig. 14. Correlation between reflected peak pressure rise time ($t_{p,r}$) and incident peak pressure rise time ($t_{p,i}$): (a) Positive; (b) Negative.

Mach number is the ratio of local flow velocity to the ambient sound speed, which determines whether Mach reflection occurs or not. Given the same incident overpressure and angle, the difference in the reflection coefficient of TNT explosions and BLEVEs is due to the Mach number. When the Mach number is higher than 1.46, a strong shock wave and Mach reflection (MR) occur, which can be addressed by von Neumann's three-shock theory (Bulat, 2016; Kobayashi et al., 1995). When the Mach number is lower than 1.46, the weak blast wave and von Neumann reflection (vNR) occur, which can be explained by von Neumann paradox (Karzova et al., 2015; Kobayashi et al., 1995; Kobayashi et al., 2000). Since BLEVE has a Mach number between 0.035 and 0.76, the weak blast wave and von Neumann reflection occur. It is worth mentioning that the incident peak overpressure is up to 345 bar in the TNT reflection coefficient chart in UFC-3–340–02, while the BLEVE reflection coefficient chart covers the incident peak overpressure up to 1 bar, which is the typical range of BLEVE pressure.

4.3. Reflected negative overpressure (P_r^-)

It is well known that negative overpressure can generate suction force and the magnitude of negative pressure from high explosive explosion is much smaller than the positive overpressure (Karlos and Solomos, 2013). Based on the 1300 sets of BLEVE data, it is found that the negative and positive reflected peak overpressures show a strong linear relationship, as given in Eq. (7). The R-square value is around 0.9, as shown in Fig. 13.

$$P_r^- = -0.26P_r^+ - 0.059 \ (bar) \tag{7}$$

4.4. Peak pressure rise time (t_p)

In addition to the reflected peak overpressures, the pressure rise rate is another essential parameter to determine the BLEVE pressure-time profile, which greatly affects the structural response. To obtain the pressure rise rate, the time to reach the peak positive and negative overpressures are defined as the peak pressure rise time (t_p^+ & t_p^-). It is well known that TNT explosion exhibits an almost instantaneous pressure rise, and the BLEVE pressure rises to the peak at a slower rate, resulting in very different structural responses because of different loading rates. BLEVE pressure rise rate can be calculated as the ratio of peak overpressure to rising time (i.e., $t_p^+ - t_a$). As shown in Fig. 14, the peak pressure rise times ($t_{p,r}$) of reflected BLEVE overpressure are very similar to the incident ones ($t_{p,i}$). Although the reflected and incident overpressure profiles have almost the same peak pressure rise time, the reflected peak pressure rise rates is greater than the incident peak pressure rise rate due to the higher values of the reflected peak

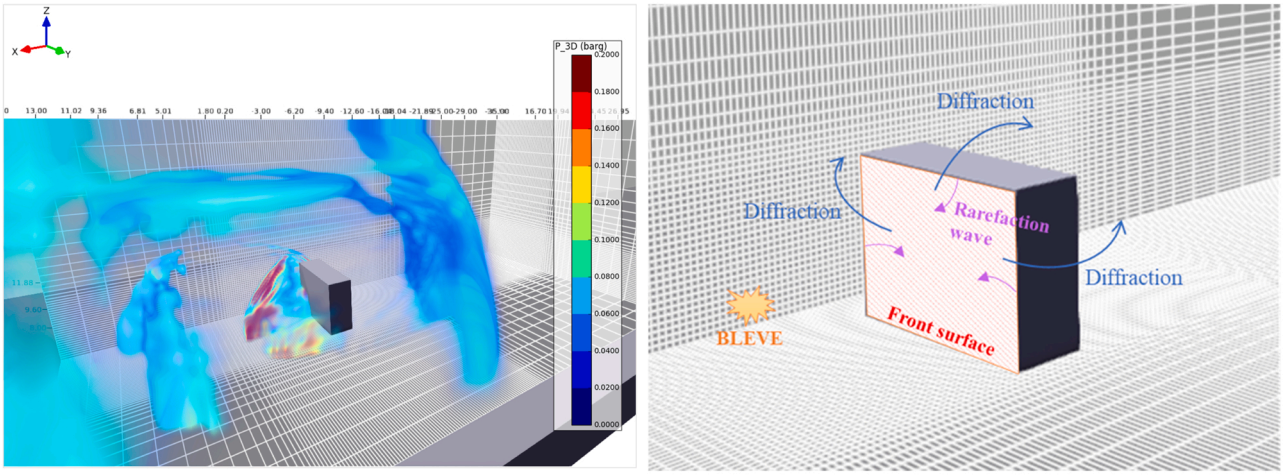

Fig. 15. BLEVE wave pressure relief from a rigid structure: (a) CFD model; (b) Schematic diagram.

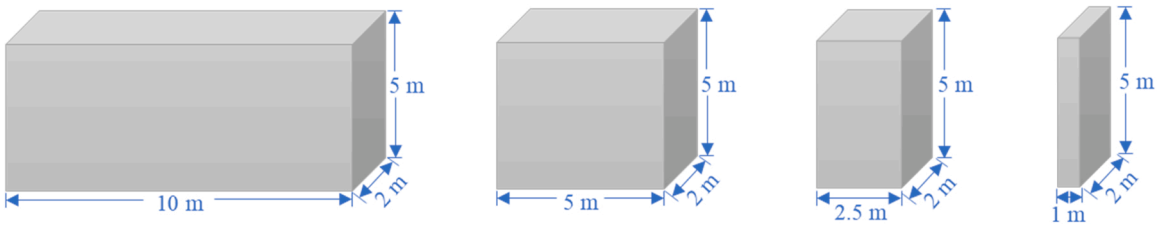

Fig. 16. Rigid structures with different widths.

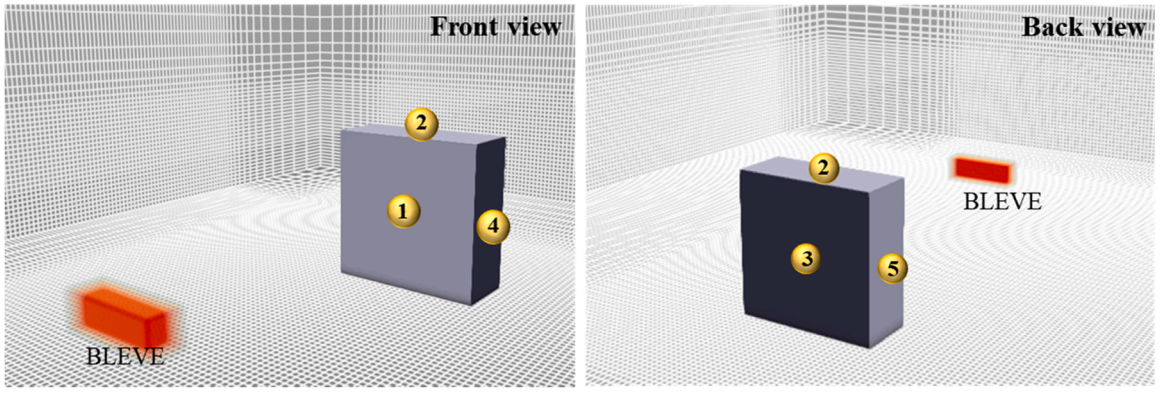

Fig. 17. Monitoring points at the centre points of different surfaces on a rigid structure.

overpressure.

5. BLEVE pressure relief

BLEVE reflection has been investigated in Section 4, and pressure relief, including wave diffraction, clearing time and reflected impulse, is discussed in this section.

5.1. BLEVE wave diffraction

The diffraction of blast waves is essential in the phenomenon of pressure relief. Pressure relief can significantly reduce the overpressure in the positive phase after the peak overpressure, thereby reducing the magnitude of the positive impulse in the reflected pressure-time profile. The dimension of the structure is a critical parameter in determining the amount of relief waves (Rickman and Murrell, 2007). Fig. 15 (a) depicts the diffracted blast waves bypassing the free edge on the top and side walls in CFD software. Meanwhile, rarefaction waves are formed in front of the structure. Fig. 15 (b) provides a schematic diagram showing the diffraction of waves around the structure and the formation of rarefaction waves.

The shortest dimension of a structure is the primary parameter dominating the pressure wave relief. Shi et al. (2007) studied the blast wave relief on structural columns, and reported that the column width greatly affected blast wave diffraction. In this study, without losing the generality, the height and the thickness of the rigid structure are fixed at 5 m and 2 m, respectively; and the width of the structure is varied from 1 m to 10 m to study the effect of structural dimensions on blast wave diffraction and reflected pressure relief, as shown in Fig. 16. Five monitoring points (MP) on the structure as shown in Fig. 17 are used to record pressure waves. The BLEVE source is assumed to be a tank with 2.7 m width, 0.86 m height and 0.86 m length. The angle of incidence between the BLEVE source and structure is set as 0°. The reflected peak overpressures on the front face of the structure are similar. However, when the structural width is small that pressure diffraction occurs before the wave is fully reflected, the reflected impulse gradually decreases with the reduced width. Fig. 18 shows the incident and reflected pressure-time profiles from MP1 to MP5, indicating the interaction of the blast wave on the front, top, sides and rear of the structure. Each monitoring point is located at the centre of the respective surface as shown in Fig. 17. Regarding reflection (i.e., MP1), when the width of the structure is 10 m and 5 m, the reflected pressure and duration are very close, i.e., the structural width and height are large enough for the pressure wave being fully reflected before diffraction. With smaller width of the structure (i.e., W_{str} = 2.5 m), the corresponding duration gradually decreases and further reduces the reflected impulse due to the diffraction of the BLEVE waves from the side edges. When the structural width is further reduced (i.e., W_{str} = 1 m), more blast waves are diffracted around the side edges of the structure, resulting in a faster release of reflected overpressure. In terms of the monitoring point on the top surface (i.e., MP2), since the blast wave propagates parallel to the free surfaces, there is nearly no reflection. Similarly, for the side surfaces (i.e., MP4 and MP5), the blast loading on the side surfaces is very similar to the BLEVE in open space at the same location. As the structural width increases, the overpressure on the side surfaces of the structure becomes slightly smaller due to the fact that the wave is partially affected by the structure. Since the angle of incidence between BLEVE centre and the structural centre is 0° (i.e., BLEVE tank has the same distance away from both sides of the structure), the overpressures on the MP4 and MP5 are the same. The overpressure on the rear surface (i.e., MP3) is remarkably lower than that of the open space due to the shadowing effects. Meanwhile, the overpressure on the rear surface of structure increases significantly with the decreased structural width. By diffracting from the side edges, more blast waves act on the rear structure with smaller width, and the diffracted waves arrive earlier when the structural width becomes smaller. Additionally, diffraction generates rarefaction waves. The effect of the pressure flow induced by the rarefaction waves on the clearing time is discussed in Section 5.2.

5.2. Clearing time (t_c)

Clearing time (t_c) is the time required to release the reflected overpressure from the affected surface, which is determined by the dimension of the structure and the speed of sound in the reflected area (S_r)

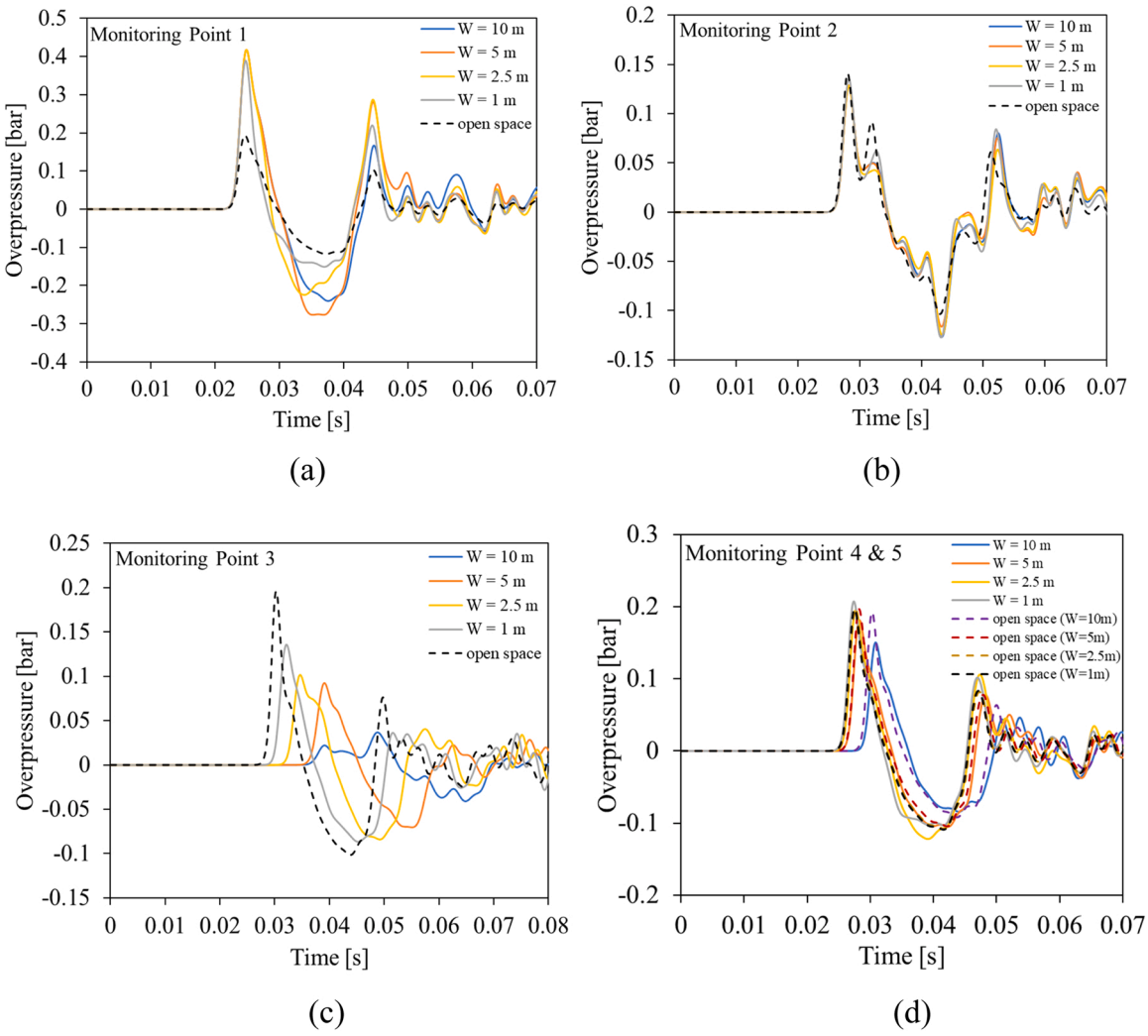

Fig. 18. Reflected pressure-time histories on a rigid structure surface at monitoring points (MP1–5).

(Lomazzi et al., 2021; UFC, 2008). The clearing effect usually begins when a blast wave arrives at the free edge of a target surface with finite dimensions (Rigby, 2014). Due to the diffraction phenomenon, the pressure flow is induced by the pressure imbalance between the higher pressure reflected wave and the lower pressure incident wave. Diffraction-generated rarefaction waves propagate along the loading surface, reducing the overpressure acting on the reflected surface and further decreasing the magnitude of the positive impulse (Rigby, 2014). When the relief wave reaches the centre of the front surface, the reflected overpressure can be fully released. As shown in Fig. 18 (a), the blast waves in front of the surface are nearly completely reflected when the structure dimensions are large enough. For instance, the blast wave is completely reflected when the width and height of the structure is 10 m and 5 m, respectively. When the width of the structure is reduced to 2.5 m, the blast wave can diffract around the side walls, as well as the top surface, resulting in pressure relief. Fig. 19 demonstrates the pressure relief in FLACS simulations. When the structural width becomes smaller, pressure waves are diffracted from the free edges of the side walls. The generated rarefaction waves create a pressure flow from high-pressure region (i.e., reflected region) to low-pressure region (i.e., rarefaction waves region), resulting in a reduction in the reflected impulse of the front wall, that is, the reflected overpressure is released.

Blast wave clearing is a complex process, and one of the reliable empirical prediction methods is the equation provided in UFC-3–340–02, as given in Eq. (8). The sound speed in BLEVE reflected region is a function of incident peak overpressure (P_s), as defined by Eq. (9) and shown in Fig. 20. The comparison of sound speed associated with TNT explosion and BLEVE is illustrated in Fig. 21, indicating BLEVE generates higher sound velocity under the same incident peak overpressure. The speed of sound depends on the conditions of the propagating medium, which is a function of the surrounding pressure and temperature. The sound speed increases with the rising local pressure or temperature (Cullis, 2001). TNT can explode at ambient pressure, while BLEVE occurs at high temperature and high pressure since the fluid in the BLEVE tank needs to be liquefied under high pressure. Due to the higher failure pressure of BLEVEs, the sound speed in BLEVEs is higher than that of TNT explosions at a similar incident peak overpressure. The clearing time is inversely proportional to the sound velocity in the reflected region. Given the same incident overpressure, the sound speed of BLEVE in a reflected zone is higher than that of TNT explosions, indicating a shorter clearing time.

$$t_c = \frac{4S}{(1+R)S_r} \tag{8}$$

where clearing distance S [m] = the shortest distance measured between the point of interest, e.g., centre of the front wall to the top or side of the structure, whichever is smaller;.

$R = S/G$, where G [m] is the largest distance between the point of interest to the top or side of the structure, whichever is larger; S_r [m/s]= sound speed in the reflected region, can be calculated by

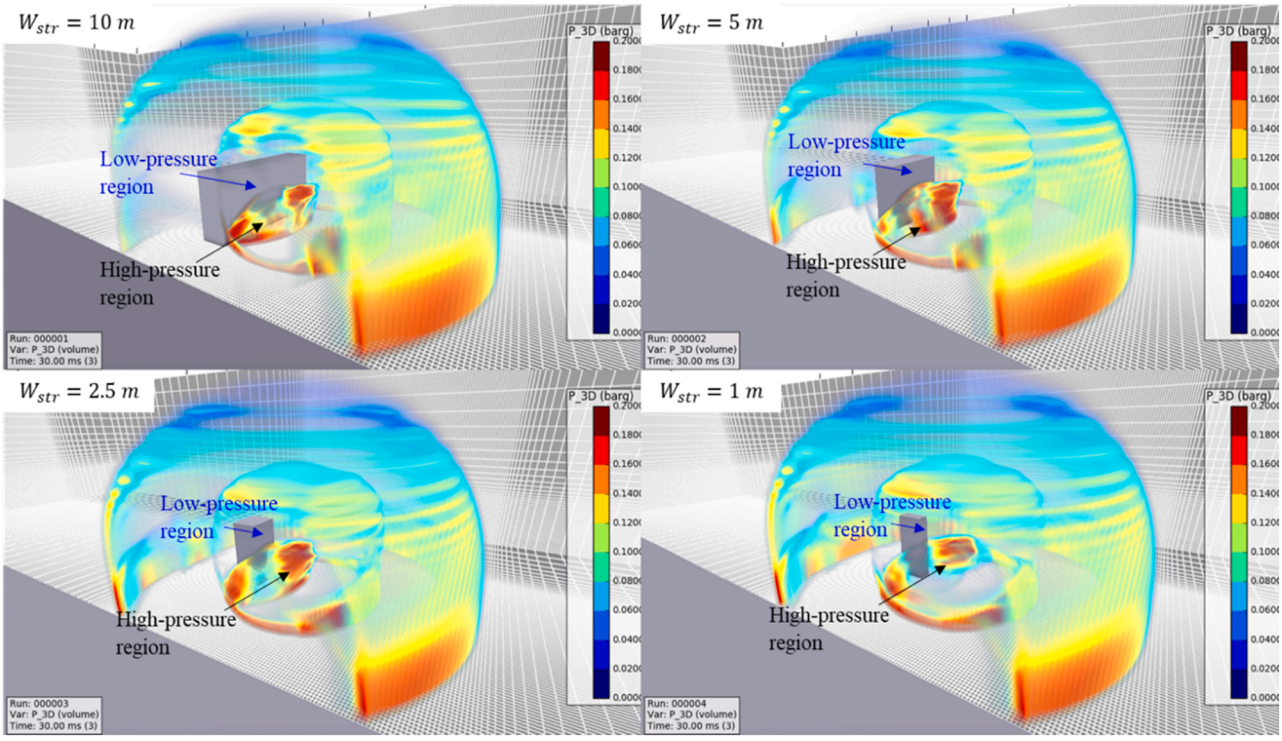

Fig. 19. Pressure relief in FLACS simulation.

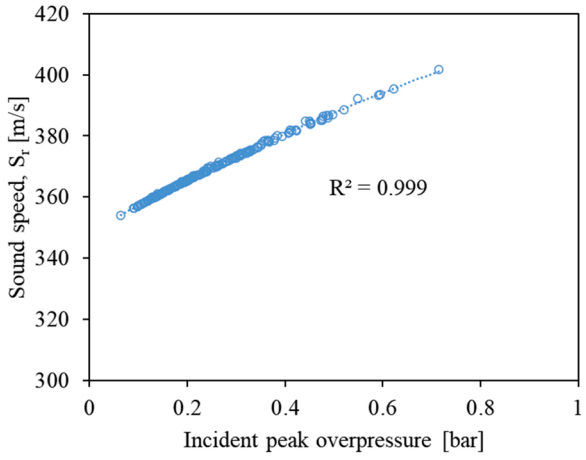

Fig. 20. Sound speed in the BLEVE reflected region.

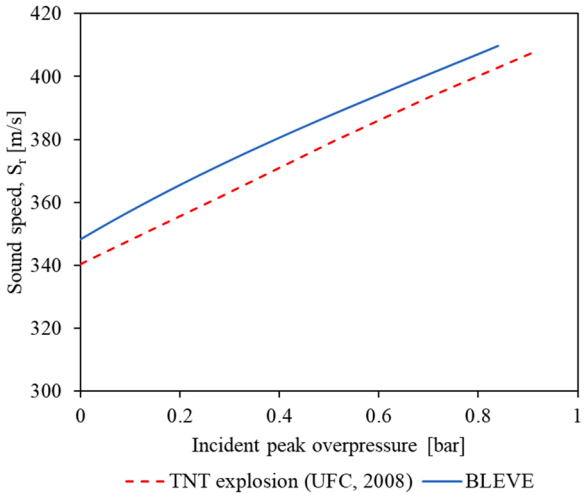

Fig. 21. Comparison of sound velocity in the reflection regions of TNT explosion (UFC, 2008) and BLEVE.

$$S_r = -20.39P_s^2 + 88.05P_s + 348.69 \quad (9)$$

where P_s [bar] = incident peak overpressure.

5.3. Reflected impulse (I_r)

In addition to reflected peak overpressure, reflected impulse (I_r) is another essential parameter to characterize the blast load on a structure (Tyas et al., 2011). By combining the blast overpressure and impulse on a specific structural element, the pressure-impulse diagram can be generated to assess the level of structural damage (Baker et al., 1983). Blast impulse is an integral time function of overpressure. Due to the limited structure size, the pressure relief phenomenon has a further effect on the reflected impulse, as it can determine how much overpressure is cleared. A portion of incident waves is diffracted along the free edges instead of completely reflected, causing partial blast waves to be cleared and lower reflected impulse. Fig. 22 shows an ideal model of non-cleared and cleared reflected pressure. The scenario with pressure relief is different from the case of complete reflection, and the cleared pressure decays linearly from the peak reflected overpressure to the stagnant overpressure (i.e., incident overpressure + drag coefficient × dynamic overpressure) within the clearing time (t_c) (Rigby, 2014). The reflected impulse results are extracted from 650 sets of BLEVE cases by varying BLEVE sources and structural dimensions. As shown in Fig. 23, the BLEVE reflected impulse (I_r) is determined by incident impulse (I_i). The R-square value of the linear fitting is around 0.96, and the fitting formula is given as follows:

$$I_r = 2.17I_i - 14.53 \ (Pa{\cdot}s) \quad (10)$$

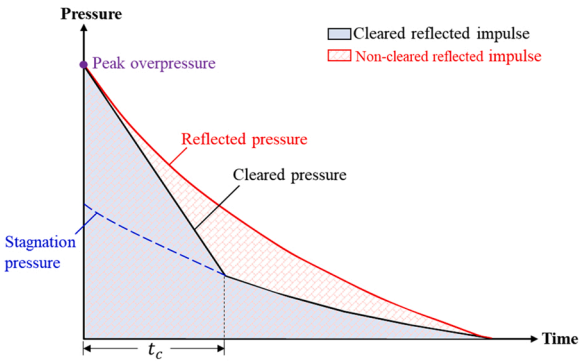

Fig. 22. Reflected impulse (I_r) (UFC, 2008).

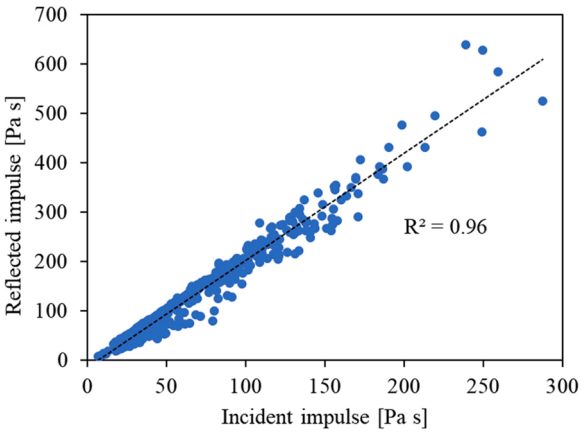

Fig. 23. Correlation between the reflected impulse (I_r) and incident impulse (I_i) at the centre of the front surface.

6. Example of application

To predict the BLEVE reflected peak overpressure and impulse on the front surface of a rigid structure, the aforementioned results can be used in combination with the BLEVE overpressure in open space proposed by the authors in a previous study (Wang et al., 2022b). An example is given in this section to demonstrate the prediction process. The previous study developed empirical models to predict BLEVE peak overpressure and impulse occurring in open space. When a BLEVE wave acts on a structure, the reflected peak overpressure can be obtained using the proposed reflection coefficient charts (i.e., Fig. 11), and the reflected impulse can be determined by using Eq. (10) with the incident impulse.

BLEVE test No. 02–1 of Birk et al. (2007) was employed as an example in the authors' previous study (Wang et al., 2022b), where the developed empirical model was used to predict the peak overpressure and impulse of BLEVE in open space. The 2 m^3 (V_{tank}) tank has a diameter of 0.953 m and a length (L_{tank}) of 2.7 m. Liquid propane is stored inside, filling to 51% of the tank's volume. BLEVE occurs under failure conditions at a pressure of 18 bar, the liquid temperature of 330 K and the vapour temperature of 334 K, respectively. Assuming that the stand-off distance is 20 m from the BLEVE centre to the rigid structure with the dimensions of 3 m width (W_{str}), 3 m height (H_{str}) and 0.4 m thickness (L_{str}), the reflected peak overpressure and impulse at the centre of a rigid structure are predicted as follows. Fig. 24 shows the schematic diagram of two cases (i.e. open space and on a rigid structure).

For the case of open space (Wang et al., 2022b), the equivalent rectangular tank's width (W_{tank}) and height (H_{tank}) can be calculated as:

$$W_{\text{tank}} = H_{\text{tank}} = \sqrt{\frac{V_{\text{tank}}}{L_{\text{tank}}}} = \sqrt{\frac{2}{2.7}} = 0.86 \ \ m$$

The peak overpressure (P_s^+ & P_s^-), durations (t_d^+ & t_d^-), arrival time (t_a), peak pressure rise time (t_p^+ & t_p^-) and impulse (I_i^+) for BLEVE in open space are calculated and listed in Table 4.

The incident angle:

$$\alpha = \arctan\left(\frac{H_{str}/2 - H_{\text{tank}}/2}{\text{stand} - \text{off distance}}\right) = arctan\left(\frac{3/2 - 0.86/2}{20}\right) = 3.06\ ^{\circ}$$

Using Fig. 11 (a), the reflection coefficient:

$$C_r = \frac{P_r^+}{P_s^+} = 2.05$$

The reflected positive peak overpressure:

$$P_r^+ = 2.05 \times 0.0813 = 0.17 \ \ bar$$

The negative peak overpressure is predicted by Eq. (7):

$$P_r^- = -0.26 \times 0.17 - 0.059 = -0.10 \ \ bar$$

Using Eq. (10), the reflected impulse:

$$I_r = 2.17 I_i - 14.53 = 59.25 \ \ Pa{\cdot}s$$

Obtaining the sound velocity in the reflection region from Fig. 20:

$$S_r = 356 \ \ m/s$$

Using Eq. (8), the clearing time:

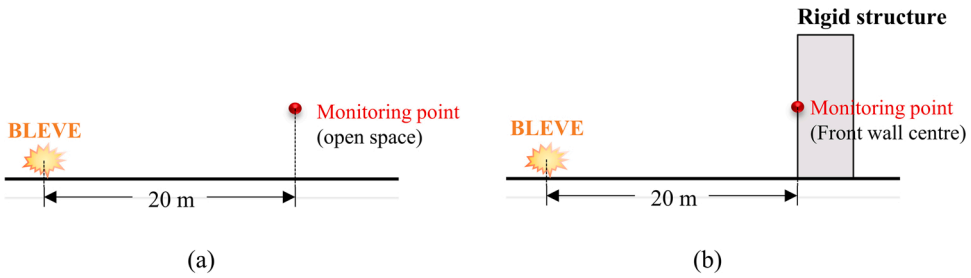

Fig. 24. Schematic diagram of two cases: (a) open space; (b) at the front centre of rigid structure.

Table 4
Predictions by using the equations in Wang et al. (2022b).

P_s^+ [bar]	P_s^- [bar]	$t_{d,i}^+$[s]	$t_{d,i}^-$[s]	$t_{a,i}$[s]	$t_{p,i}^+$[s]	$t_{p,i}^-$[s]	I_i^+[Pa • s]
0.0813	-0.0600	0.0084	0.0111	0.0488	0.0526	0.0652	34

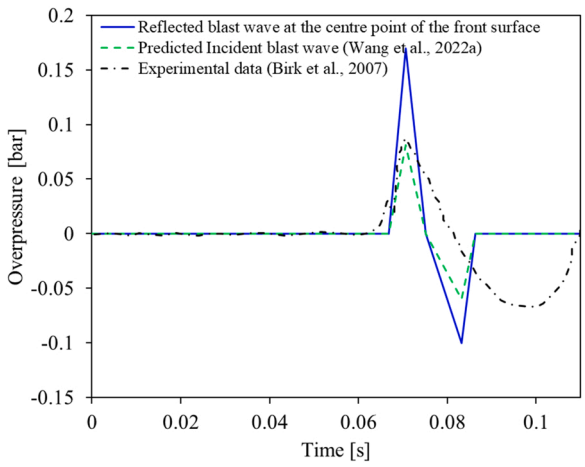

Fig. 25. Reflected and incident pressure-time histories.

$$t_c = \frac{4S}{(1+R)S_r} = \frac{4\times(3/2)}{(1+1.5/3)\times 356} = 0.011\ \ s$$

The arrival time:

$$t_{a,r} = t_{a,i} = 0.0488\ \ s$$

The reflected overpressure duration and peak pressure rise time are close to the incident ones, expressed as:

$$t^{+}_{d,r} = t^{+}_{d,i} = 0.0084\ \ s$$

$$t^{-}_{d,r} = t^{-}_{d,i} = 0.0111\ \ s$$

$$t^{+}_{p,r} = t^{+}_{p,i} = 0.0526\ \ s$$

$$t^{-}_{p,r} = t^{-}_{p,i} = 0.0652\ \ s$$

The above results indicate that clearing time is longer than the positive phase duration, implying the pressure wave is fully reflected. As shown in Fig. 25, the reflected overpressure at the centre of the front surface is presented and compared with the corresponding incident pressure-time histories, i.e., experimental data (Birk et al., 2007) and the predicted results using Wang's equation (Wang et al., 2022b).

As discussed above, the BLEVE load acting on top and side faces of the structure can be approximated by the free-field pressure waves. It should be noted that the prediction of BLEVE load on rear surface is more complicated as indicated above and is also less significant. For these reasons, BLEVE load prediction on rear face of structures is not included in this study.

7. Conclusions

In this study, a total of 1300 sets of BLEVE cases consisting of 650 in open space and 650 pressure wave-rigid structure interaction cases are simulated by using FLACS. Reflected overpressure and impulse induced by BLEVE on a rigid rectangular structure are obtained and analysed. The following conclusions can be drawn:

1. Reflection coefficient (C_r) charts for positive overpressure on a rigid structure are developed based on different angles of incidence and the incident peak overpressure in open space.
2. Von Neumann reflection rather than Mach reflection occurs in BLEVE when the angle of incidence reaches the critical incidence angle.
3. The relationship between negative reflected peak overpressure (P_r^-) and positive reflected peak overpressures (P_r^+) is proposed as Eq. (7).
4. Incident and reflected BLEVE pressure-time profiles have very similar peak pressure rise time. However, the reflected BLEVE pressure rise rate is larger than the incident one as the reflected peak overpressure is higher than the incident peak overpressure.
5. The sound speed chart of BLEVE in the reflected region is proposed to calculate the clearing time. BLEVE waves require a shorter clearing time (t_c) than shock waves from TNT explosions at similar incident peak overpressure and structural dimensions.
6. The empirical formula (10) is proposed to predict the BLEVE-induced reflected impulse (I_r) on a rigid structure.
7. The results presented in this study together with BLEVE pressure predictions reported in a previous study can be used to estimate BLEVE loads on structures.

Declaration of Competing Interest

The authors declare that they have no known competing financial interests or personal relationships that could have appeared to influence the work reported in this paper.

Acknowledgements

The authors acknowledge the financial support from the Australian Research Council (ARC) via Australian Laureate Fellowship (FL180100196).

References

A., Hutama 2017. Simulation of BLEVEs in unconfined and confined areas using FLACS. University of Stavanger Norway.
ASCE, 2010. Design of Blast-Resistant Buildings in Petrochemical Facilities (Second Edition). Task Committee on Blast Resistant Design of the Petrochemical Committee of the Energy Division of the American Society of Civil Engineers.
Baker, W.E., Cox, P., Westine, P., Kulesz, J., Strehlow, R., 1983. Explosion hazards and evaluation. Elsevier,, New York.
Balke, C., Heller, W., Konersmann, R., Ludwig, J., 1999. Study of the Failure Limits of a Railway Tank Car Filled with Liquefied Petroleum Gas Subjected to an Open Pool Fire Test. Federal Institute for Materials Research and Testing (BAM),, Berlin, Germany.
Bariha, N., Srivastava, V.C., Mishra, I.M., 2017. Theoretical and experimental studies on hazard analysis of LPG/LNG release: a review. Rev. Chem. Eng. 33, 387–432.
Betteridge, S., Phillips, L., 2015. Large scale pressurised LNG BLEVE experiments. Inst. Chem. Eng. Symp. 353–364.
Birk, A.M., Davison, C., Cunningham, M., 2007. Blast overpressures from medium scale BLEVE tests. J. Loss Prev. Process Ind. 20, 194–206.
Bulat, P.V., 2016. The history of the study of shock wave's mach reflection from the wedge. Int. Electron. J. Math. Educ. 11, 1151–1162.
CCPS, 2011. Guidelines for vapor cloud explosion, pressure vessel burst, BLEVE, and flash fire hazards. Wiley Online Libr,, p. 456.
CNN-news, 2018. Three dead in Bologna highway gas tanker explosion. ⟨https://pantagraph.com/video/featured/three-dead-in-bologna-highway-gas-tanker-explosion/article_7f1811ac-8cbf-5899-9039-3080bfbaeaee.html⟩.
CSB, 2008. CSB Safety Video: Anatomy of a Disaster. ⟨https://www.youtube.com/watch?v=XuJtdQOU_Z4&t=204s⟩.
Cullis, I., 2001. Blast waves and how they interact with structures. BMJ Mil. Health 147, 16–26.
D., Johnson, M., Pritchard, 1990. Large scale experimental study of boiling liquid expanding vapour explosions (BLEVEs) Gastech 90 Int. LNG/LPG Conf. Exhib.
Eckhoff, R.K., 2014. Boiling liquid expanding vapour explosions (BLEVEs): a brief review. J. Loss Prev. Process Ind. 32, 30–43.
Gexcon, 2022. FLACS-CFD v22.1r2 User's Manual, Norway.
Green-Book, T., 1992. Method for the determination of possible damage to people and objects resulting from releases of hazardous materials. CPR 16E. TNO Neth. Organ. Appl. Sci. Res.
Hansen, O.R., Kjellander, M., 2016. CFD modelling of blast waves from BLEVEs. Chem. Eng. Trans. 48, 199–204.
Hao, H., Hao, Y., Li, J., Chen, W., 2016. Review of the current practices in blast-resistant analysis and design of concrete structures. Adv. Struct. Eng. 19 (8), 1193–1223.
Johnson-Yurchak, J., 2020. Validation of the Mach Stem Triple Point. Lawrence Livermore National Lab.(LLNL), Livermore. CA (United States); California Polytechnic State Univ. (CalPoly). San Luis Obispo,, CA (United States).
Kadatec, 2017. LPG Road. Tankers ISO Tank. Contain. V9, 092017.
Karlos, V., Solomos, G., 2013. Calculation of blast loads for application to structural components. Publications Office of the European Union,, Luxembourg.
Karzova, M.M., Khokhlova, V.A., Salze, E., Ollivier, S., Blanc-Benon, P., 2015. Mach stem formation in reflection and focusing of weak shock acoustic pulses. J. Acoust. Soc. Am. 137, EL436–EL442.

Kobayashi, S., Adachi, T., Suzuki, T., 1995. Examination of the von Neumann paradox for a weak shock wave. Fluid Dyn. Res. 17, 13–25.
Kobayashi, S., Adachi, T., Suzuki, T., 2000. Non-self-similar behavior of the von Neumann reflection. Phys. Fluids 12, 1869–1877.
Li, J., Hao, H., 2019. Numerical and analytical prediction of pressure and impulse from vented gas explosion in large cylindrical tanks. Process Saf. Environ. Prot. 127, 226–244.
Li, J., Hao, H., 2020. Numerical study of medium to large scale BLEVE for blast wave prediction. J. Loss Prev. Process Ind. 65, 104–107.
Li, J., Hao, H., 2021. Numerical simulation of medium to large scale BLEVE and the prediction of BLEVE's blast wave in obstructed environment. Process Saf. Environ. Prot. 145, 94–109.
Li, J., Li, Q., Hao, H., Li, L., 2021. Prediction of BLEVE blast loading using CFD and artificial neural network. Process Saf. Environ. Prot. 149, 711–723.
Liu, Z., Ma, Y., Ren, Y., Li, M., Li, P., Wan, S., 2020. Experimental and numerical study on the gas explosion in urban regulator station. J. Beijing Inst. Technol. 29, 195–208.
Lomazzi, L., Giglio, M., Manes, A., 2021. Analysis of the blast wave–structure interface phenomenon in case of explosive events. IOP Conference Series: Materials Science and Engineering. IOP Publishing,, 012083.
Ngo, T., Mendis, P., Gupta, A., Ramsay, J., 2007. Blast loading and blast effects on structures-an overview. Electron. J. Struct. Eng. 7, 76–91.
Rickman, D.D., Murrell, D.W., 2007. Development of an improved methodology for predicting airblast pressure relief on a directly loaded wall, 129. J. Press. Vess. Technol.,, pp. 195–204.
Rigby, S.E., 2014. Blast wave clearing effects on finite-sized targets subjected to explosive loads. Univ. Sheff.
Rigby, S.E., Tyas, A., Bennett, T., 2012. Single-degree-of-Freedom response of finite targets subjected to blast loading - the influence of clearing. Eng. Struct. 45, 396–404.
Rigby, S.E., Fay, S.D., Tyas, A., Warren, J.A., Clarke, S.D., 2015. Angle of incidence effects on far-field positive and negative phase blast parameters. Int. J. Prot. Struct. 6, 23–42.
S.B. Janney 2007 Blast resistant design of steel structures Univ. Tenn. Knoxv.
Shi, Y., Hao, H., Li, Z.-X., 2007. Numerical simulation of blast wave interaction with structure columns. Shock Waves 17 (1), 113–133.
Shin, J., Whittaker, A.S., Aref, A.J., Cormie, D., 2017. Reflection coefficients and reflected scaled impulses from detonations of high explosives as a function of angle of incidence. J. Struct. Eng. 143, 04017043.
Tyas, A., Warren, J.A., Bennett, T., Fay, S., 2011. Prediction of clearing effects in far-field blast loading of finite targets. Shock Waves 21, 111–119.
UFC, 2008. Unified Facilities Criteria: structures to resist the effects of accidental explosions (UFC 3–340-02). US Department of Defense, Washington, DC.
Ustolin, F., Tolias, I.C., Giannissi, S.G., Venetsanos, A.G., Paltrinieri, N., 2022. A CFD analysis of liquefied gas vessel explosions. Process Saf. Environ. Prot. 159, 61–75.
Wang, Y., Li, J., Hao, H., 2022a. A state-of-the-art review of experimental and numerical studies on BLEVE overpressure prediction. J. Loss Prev. Process Ind. 80, 104920.
Wang, Y., Li, J., Hao, H., 2022b. Development of efficient methods for prediction of medium to large scale BLEVE pressure in open space. Process Saf. Environ. Prot. 161, 421–435.
Xu, R., Chen, L., Fang, Q., Zheng, Y., Li, Z., Cao, M., 2021. Protective effects of gabion wall against blast waves from large TNT-equivalent explosions. Eng. Struct. 249, 113389.